Neuronal Hyperpolarization-Activated Pacemaker Channels Drive Neuropathic Pain

Sandra R. Chaplan, Hong-Qing Guo, Doo Hyun Lee, Lin Luo, Changlu Liu, Chester Kuei, Alexander A. Velumian, Matthew P. Butler, Sean M. Brown, and Adrienne E. Dubin

Neuroscience, Johnson & Johnson Pharmaceutical Research and Development, San Diego, California 92121

Neuropathic pain is a common and often incapacitating clinical problem for which little useful therapy is presently available. Painful peripheral neuropathies can have many etiologies, among which are trauma, viral infections, exposure to radiation or chemotherapy, and metabolic or autoimmune diseases. Sufferers generally experience both pain at rest and exaggerated, painful sensitivity to light touch. Spontaneous firing of injured nerves is believed to play a critical role in the induction and maintenance of neuropathic pain syndromes. Using a well characterized nerve ligation model in the rat, we demonstrate that hyperpolarization-activated, cyclic nucleotide-modulated (HCN) "pacemaker" channels play a previously unrecognized role in both touch-related pain and spontaneous neuronal discharge originating in the damaged dorsal root ganglion. HCN channels, particularly HCN1, are abundantly expressed in rat primary afferent somata. Nerve injury markedly increases pacemaker currents in large-diameter dorsal root ganglion neurons and results in pacemaker-driven spontaneous action potentials in the ligated nerve. Pharmacological blockade of HCN activity using the specific inhibitor ZD7288 reverses abnormal hypersensitivity to light touch and decreases the firing frequency of ectopic discharges originating in Aβ and Aδ fibers by 90 and 40%, respectively, without conduction blockade. These findings suggest novel insights into the molecular basis of pain and the possibility of new, specific, effective pharmacological therapies.

Key words: **neuropathic pain; ectopic discharge; dorsal root ganglion; HCN channel; pacemaker channel; spinal nerve ligation; I_h**

Introduction

Patients with peripheral nerve injuries frequently complain of painful spontaneous sensations, chiefly constant and burning or intermittent and lancinating in quality. Pain evoked by normally innocuous stimuli is common: in particular, light touch may evoke an excruciating sensation termed allodynia. Spontaneous pain and allodynia may be the most clinically troublesome sensations, although increased sensitivity to pressure and to thermal stimuli are also described.

Spontaneous sensations likely result from ongoing neural activity, and allodynia and hyperalgesia are attributed to both hypersensitivity of sensory pathways and miscoding of sensory information (Rappaport and Devor, 1990). Although a prominent role of CNS sensory processing is likely in this pathology, discharges from the injured peripheral nerve are believed to be critical to the initiation and maintenance of neuropathic pain syndromes.

In neuropathic pain, unlike acute pain, unmyelinated fibers, although classically considered "nociceptive," may play a limited role. In the rat, neonatal capsaicin treatment to abolish nearly all unmyelinated fibers does not reduce the pain behaviors associated with a subsequent nerve injury (Okuse et al., 1997). Of note, Aβ fibers, which are normally associated with nonpainful light touch, vibration, and proprioceptive senses, have been shown to transmit the sensation of allodynia (Shir and Seltzer, 1990).

Acute nerve transection causes a burst of firing and then a "silent period" of ~12 hr, followed by the appearance of abnormal spontaneous discharges (Govrin-Lippmann and Devor, 1978). These discharges emanate from both the site of injury and the dorsal root ganglion (DRG) itself, typically have strong rhythmic components, and originate mainly in both large- and medium-sized DRG neurons associated with Aβ and Aδ fibers, respectively (Burchiel, 1984; Kajander and Bennett, 1992).

The spontaneity and regularity of firing patterns strongly suggest the possibility of automaticity attributable to a pacemaker-driven phenomenon. Pacemaker currents (I_h) have been reported previously in DRG neurons, particularly large neurons (Mayer and Westbrook, 1983; Scroggs et al., 1994). In addition, previous *in vitro* work is supportive of a role for I_h in hyperexcitability of the damaged peripheral nerve (Yagi et al., 2000). The family of ion channels responsible for I_h has been identified recently (Santoro et al., 1997, 1998; Ludwig et al., 1998). These hyperpolarization-activated, cation-nonselective, cyclic nucleotide-modulated (HCN) channels are permeable to both K^+ and Na^+ and underlie depolarizations that modulate the rhythmic generation of action potentials (APs), contribute to the resting membrane potential (RMP), and modify the waveform of propagated synaptic and generator potentials (Pape, 1996). HCN channels have significant homology with 6-transmembrane-domain potassium channels and possess an intracellular cyclic nucleotide-binding domain. The four presently known family members (HCN1–4) share substantial homology but differ significantly in their activation kinetics and re-

Received Aug. 20, 2002; revised Nov. 23, 2002; accepted Dec. 5, 2002.

This work was entirely supported by Johnson & Johnson Pharmaceutical Research and Development. We thank Curt Mazur and Brian Lord for assistance with the pharmacokinetic study, and Dr. Geoffrey Abbott for helpful discussions during manuscript preparation.

Correspondence should be addressed to Dr. S. R. Chaplan, Johnson & Johnson Pharmaceutical Research and Development, 3210 Merryfield Row, San Diego, CA 92121. E-mail: schaplan@prdus.jnj.com.

A. A. Velumian's present address: Toronto Western Hospital, Toronto Western Research Institute, McLaughlin Pavilion, Room 12-411, 399 Bathurst Street, Toronto, Ontario M5T 2S8 Canada.

M. P. Butler's present address: Department of Integrative Biology, University of California, Berkeley, 3060 Valley Life Sciences Building 3140, Berkeley, CA 94720-3140.

 0270-6474/03/231169-10$15.00/0

sponsiveness to cAMP (Santoro and Tibbs, 1999; Ishii et al., 2001; Kaupp and Seifert, 2001). We tested the hypothesis that abnormal activity of neuronal pacemaker channels contributes to pathological spontaneous electrical behavior, abnormal RMP, and hypersensitivity of primary afferent fibers to ordinarily non-noxious sensory stimuli. As part of our effort to distinguish the molecular basis of the observed changes in I_h after nerve injury, we characterized the function of expressed full-length clones of human HCN1 (hHCN1) and human HCN3 (hHCN3).

Materials and Methods

Animals. The Institutional Animal Care and Use Committee of Johnson & Johnson Pharmaceutical Research and Development approved all protocols. Male Sprague Dawley rats (Harlan, Indianapolis, IN) were housed in cages with corncob bedding, a reverse 12 hr light/dark cycle, and *ad libitum* access to chow and water.

Surgical neuropathy and behavior. For behavior studies, the left lumbar fifth (L5) and L6 spinal nerves of 100–150 gm rats were exposed (sham) or firmly ligated using 6-0 silk suture [spinal nerve ligation (SNL)] under isoflurane/oxygen anesthesia as described previously (Kim and Chung, 1992). Calibrated von Frey filaments (0.41, 0.63, 1.0, 1.58, 2.51, 4.07, 6.31, 10, 15.8 gm) (Stoelting, Wood Dale, IL) were used to document the 50% threshold for hindpaw withdrawal as described previously (Chaplan et al., 1994). For *ex vivo* electrophysiological studies, L4 and L5 spinal nerves were ligated versus exposed, as described previously (Lee et al., 1999).

Intrathecal cannulation. Under isoflurane/oxygen anesthesia, a sterile 8.5 cm catheter of polyethylene tubing was introduced at the atlanto-occipital junction and threaded to the lumbar enlargement; the cephalad end was exteriorized and capped as described previously (Yaksh and Rudy, 1976). After 1 week of recovery, drugs were administered in a volume of 10 μl followed by 10 μl of saline flush.

Drugs and reagents. ZD7288 (molecular weight 292.81; Tocris Cookson, Ellisville, MI) was diluted in sterile 0.9% saline and administered by the specified routes in the various experiments. All other reagents were from Sigma-Aldrich unless stated otherwise.

Pharmacokinetics. Four rats (~300 gm) were given ZD7288 (10 mg/kg, i.p.) prepared immediately before injection in a volume of 1 ml/kg. Tail vein blood was sampled in 250 μl heparinized aliquots with a 23 gauge needle at time points matching behavioral determinations (15, 30, 60, 120, 240, 360, and 1440 min). Plasma was separated from samples by centrifugation and frozen at −20°C until liquid chromatography and tandem mass spectometry analysis. Pharmacokinetic parameters were determined using the WinNonlin software package (Pharsight Corporation, Mountain View, CA).

Ex vivo *electrophysiology.* The left L4 or L5 dorsal root, DRG, and nerve were excised in continuity 1–3 weeks after tight ligation and placed in a two-compartment recording chamber. *Ex vivo* recording of single spontaneously active units, distinguished by amplitude and waveform, was performed at room temperature (Lee et al., 1999). Fiber types were classified according to conduction velocity: >14 m/sec for Aβ, 2–14 m/sec for Aδ, and <2 m/sec for C fibers (Harper and Lawson, 1985; Waddell and Lawson, 1990; Ritter and Mendell, 1992).

RNA quantification. One week after surgery, total RNA was extracted from left L5/L6 for each rat (RNEasy, Qiagen, Valencia, CA). Conventional first-strand cDNA synthesis was performed on 1/10 of the yield using Superscript II (Invitrogen, Carlsbad, CA); 1/16 of the resulting preparation served as template per PCR reaction. Samples were analyzed simultaneously using an iCycler (Bio-Rad, Hercules, CA), with *Taq*PCR Master Mix (Qiagen) containing 1:50,000 SybrGreen (Molecular Probes, Eugene, OR). Gene-specific primers (Genset, La Jolla, CA) were as follows: HCN1: bases 308–329 and 548–570 (5′ amplicon) and 2391–2413 and 2589–2620 (3′ amplicon) of GenBank accession number 247450 (NM 053375); HCN2: 332–349 and 464–492 of AF247451; HCN3: 140–157 and 318–337 of AF247452 (NM 053685); HCN4: 589–610 and 777–805 of AF247453; and cyclophilin A: 157–182 and 496–521 of NM 017101. HCN PCR amplicons spanned large introns to preclude genomic DNA amplification. Products were cloned into pCR4-TOPO vector (Invitrogen) and sequenced. Relative fluorescence was compared during the log-linear phase of amplification, and copy number was calculated on the basis of plasmid standard dilutions. Fractional cyclophilin recovery was computed by dividing all cyclophilin values by the value for the sample with maximum recovery. Relative normalization was performed by dividing HCN copy numbers by the fractional retrieval of cyclophilin for each respective sample.

Antibodies. Glutathione *S*-transferase fusion proteins representing rHCN1 amino acids 842–910 or rHCN3 amino acids 712–780 were generated using standard techniques. Purified fusion proteins were submitted to R&R Rabbitry (Stanwood, WA). Anti-HCN2 was purchased from Alomone Labs (Jerusalem, Israel).

In situ *hybridization and immunohistochemistry.* Left (injured) and right (uninjured) fifth lumbar DRGs were embedded in the same cryomold and processed simultaneously. A digoxigenin-based detection system was used for *in situ* hybridization (ISH) (Braissant and Wahli, 1998). Labeled antisense and sense cRNA probes corresponded to bases 2391–2602, 1448–1880, 1907–2232, and 3459–3815 of sequences with GenBank accession numbers AF247450 (NM 053375) (HCN1), AF247451 (HCN2), AF247452 (NM 053685) (HCN3), and AF247453 (HCN4), respectively.

For immunohistochemistry, postfixed sections were blocked in 5% normal goat serum and then incubated with rabbit anti-HCN antibodies overnight at 4°C (anti-HCN1, 1:2000; anti-HCN2, 1:500; anti-HCN3, 1:1000). After secondary antibody application, sections were developed with a Vectastain Elite ABC kit (Vector Laboratories, Burlingame, CA) and visualized with 3,3′-diaminobenzidine-tetrahydrochloride. Negative controls consisted of peptide or fusion protein preabsorption as well as omission of primary antibodies.

Western blot analysis. Human embryonic kidney (HEK) 293 and HEK-tsA201 cells stably expressing recombinant hHCN1 or hHCN3, respectively, or DRGs were disrupted in lysis buffer (75 mM Tris-HCl, pH 7.2, 200 mM NaCl, 1% Tween-100, 1 mM EDTA, 1 mM DTT with protease inhibitor). Lysates were separated on SDS-PAGE gels and transferred to nitrocellulose membranes. After blocking with 5% nonfat dry milk in TBST (20 mM Tris-HCl, pH 7.5, 150 mM NaCl, 0.05% Tween-20), membranes were incubated with rabbit anti-HCN1 or -HCN3 (1:3000 and 1:2000) in 2% nonfat dry milk in TBST overnight at 4°C. Membranes were washed, incubated with goat anti-rabbit antibody (HRP labeled) in TBST with nonfat dry milk and detected with ECL reagents (Amersham Biosciences, Arlington Heights, IL). Blots were scanned and band densities were compared using Un-Scan-IT software for the Macintosh (Silk Scientific, Orem, UT).

Cloning of human HCN1 cDNA. The rat HCN1 coding region sequence (AF247450) was used to query the human genome draft sequence to identify putative human HCN1 translation start and stop sites. Two primers, forward 5′-ACGTAAGCTTGCCACCATGGAAGGAGGCGGCAAGCCAAC-3′ and reverse 5′-ACGTAGGCGCCGCTCATAAATTTGAAGCAAATCGTGGCT-3′, were used to PCR amplify the human HCN1 coding region using human spinal cord cDNA as template. A 2.7 kb PCR fragment was cloned into the expression vectors pGEMHE (Liman et al., 1992) and pCDNA3.1 Zeo (Invitrogen), and the complete insert region was sequenced for confirmation.

Cloning of human HCN3 cDNA. The rat HCN3 cDNA sequence (AF247452) was used to query GenBank to identify a partial cDNA encoding KIAA1535 protein (AB040968) with high homology to the 3′ end of rat HCN3. Two primers, 5′-CGGAAGCGCTCCGAGCCAAGTCCAGGCAGCAGT-3′ (designed from KIAA1535) and 5′-CCATCCTAATACGACTCACTATAGGGC-3′ (an adaptor) were synthesized to PCR amplify the 5′ end of human HCN3 using human brain Marathon-ready cDNA (Clontech, Palo Alto, CA) as template. The resulting amplicon was sequenced to obtain the 5′ end sequence of human HCN3. Two primers, forward 5′-ATCAAAGCTTGCCACCATGGAGGCAGAGCAGCGGCCGGCGG-3′ and reverse 5′-ACGTACGCGGCCGCTTACATGTTGGCAGAAAGCTGGAGAC-3′, were used to amplify the human HCN3 full coding region. The resulting 2.3 kb PCR fragment was cloned into pGEMHE and pCDNA3.1 Zeo and verified by sequencing.

Patch-clamp studies. Aseptically excised sham and SNL ganglia were collected in ice-cold Tyrode's containing 50 mg/l gentamicin, incubated

in Tyrode's containing 2 mg/ml collagenase and 1 mg/ml protease for 45 min at 37°C with 5% CO_2, followed by washes in Tyrode's and gentle dissociation by trituration in 1 ml of DMEM with 10% fetal bovine serum. Cells were plated on poly-D-lysine-coated coverslips and maintained at 37°C. Whole-cell patch-clamp recordings (Dubin et al., 1999b) were made at room temperature, 6–48 hr after plating, from single L5 DRG neurons with diameter >42 μm. The extracellular bath was a modified Tyrode's solution containing (in mM): 145 NaCl, 4 KCl, 1 $CaCl_2$, 1.2 $MgCl_2$, 10 dextrose, 10 Na-HEPES, pH 7.3. Recording electrodes had resistances of 1–2 MΩ when filled with intracellular saline containing (in mM): 130 K-gluconate, 10 NaCl, 3 $MgCl_2$, 10 HEPES, 2 Mg-ATP, 0.1 EGTA, pH 7.3. Currents were normalized to cell size using total membrane capacitance ($C_{m)}$ (Dubin et al., 1999a). C_m was 139 ± 6 pF ($n = 52$) and 115 ± 6 pF ($n = 39$) for SNL and sham controls, respectively. Hyperpolarizing steps were made from either −44 or −54 mV to more negative potentials beginning at −64 mV in increments of 10 mV. I_h was measured as the difference between the initial baseline current at the end of the capacitative transient and the steady-state current at the end of ≥2 sec test pulses and was similar to the steady-state Cs^+-sensitive current measured at the end of the test pulse. The voltage dependence of current activation was fit by a Boltzmann function using GraphPad Prism (San Diego, CA). The kinetics of current activation were determined using Chebyshev with a four-point smoothing filter in CLAMPFIT (Axon Instruments, Union City, CA). The currents were usually best described by a two-exponential fit.

Expression studies. Xenopus oocytes were injected with *in vitro* transcribed cRNA for hHCN1 and hHCN3 (1 ng each) and recorded 1–8 d later by conventional two-electrode voltage clamp using previously described methods (Dubin et al., 1999b) using the PClamp8 program suite (Axon Instruments).

Statistics. Results are stated as mean ± SEM. Paw thresholds and percentage inhibition of single fibers *ex vivo* were compared using two-way repeated ANOVA with Dunnett's *post hoc* comparisons. Quantitative PCR results were compared using unpaired *t* tests. Student's *t* test was used to compare I_h parameters and RMP in sham and SNL DRG neurons. $p < 0.05$ was considered significant.

Results

We used a well characterized rat nerve injury paradigm, the spinal nerve ligation model (Kim and Chung, 1992), to study the role of I_h in tactile allodynia. We tested whether ZD7288, a specific blocker of I_h (but nonselective among the four known HCN channels), could modify neuropathic pain behavior. ZD7288 dose-dependently suppressed the tactile allodynia exhibited by awake SNL rats without adverse effects, with a maximum efficacy of 78.8 ± 13.1% at the highest tolerated dose of 10 mg/kg, i.p. ($n = 7–8$ per group) (Fig. 1*a*). At a higher dose (20 mg/kg), signs of sedation were seen.

A parallel pharmacokinetic study emphasized the wide tissue distribution of ZD7288 and the low plasma concentration required to suppress allodynia *in vivo*. The maximum plasma concentration of ZD7288 attained was 3.6 ± 0.3 μM, between 15–30 min after dosing. The half-life was 1.9 ± 0.1 hr. At 60 min, when maximum anti-allodynic efficacy was seen, the mean plasma concentration was 1.3 ± 0.1 μM. The volume of distribution was large, at 6.03 ± 0.37 l, which is indicative of extensive partitioning into tissues.

Unlike systemic administration, administration via the lumbar intrathecal route (i.t.) had no effect on allodynia up to the maximally tolerated dose of 50 μg (Fig. 1*c*) (estimated CSF concentration in excess of 500 μM). Beyond this dose, hindlimb motor deficits were produced, strongly suggesting that the anti-allodynic effect of ZD7288 is not on the spinal cord or dorsal roots. These observations are compatible, however, with an effect on either the peripheral nerve or the DRG, because the DRG lies outside the blood–brain barrier (Olsson, 1968).

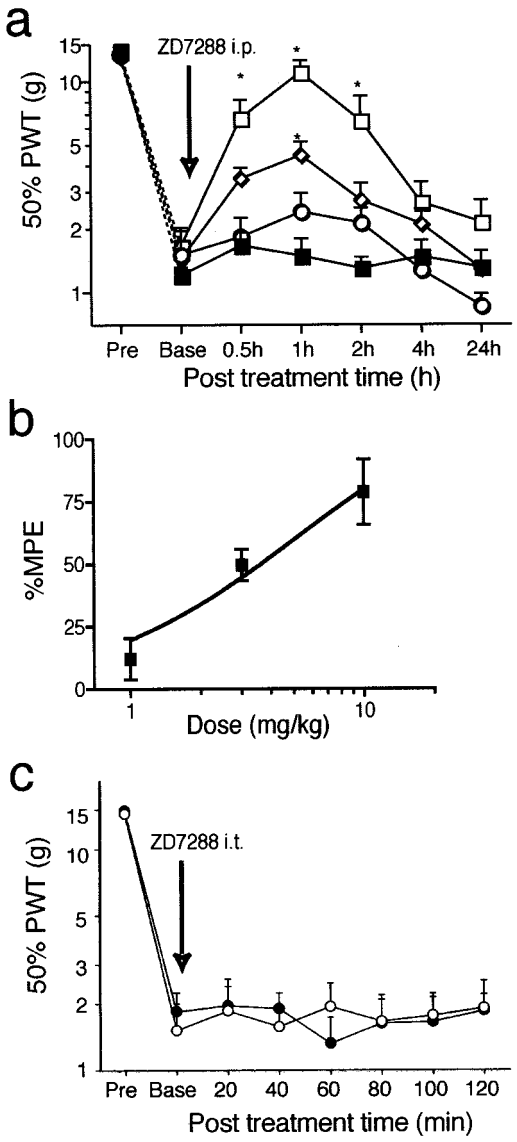

Figure 1. The HCN antagonist ZD7288 reverses neuropathic pain behavior. *a*, One week after SNL, rats received equivalent volumes of intraperitoneal saline (■), 1 mg/kg ZD7288 (○), 3 mg/kg ZD7288 (◇), or 10 mg/kg ZD7288 (□) after baseline assessment of tactile allodynia with von Frey hairs. The redacted time course of allodynia suppression is illustrated: *y*-axis = 50% paw withdrawal threshold (*PWT*) (normal = 15 gm; allodynia = lower threshold values). At 10 mg/kg, near complete suppression of allodynia is seen. *$p < 0.05$, one-way ANOVA with Dunnett's multiple comparisons; $n = 7–8$ per group. *b*, The dose–response curve for ZD7288 from *a*: *y*-axis: percentage of maximum possible effect (*MPE*) (15 gm threshold = 100% allodynia suppression; no change from pre-drug baseline = 0%). The ED_{50} for allodynia suppression is ~3 mg/kg. *c*, Lumbar intrathecal administration of ZD7288, 50 μg (●), had no effect on SNL-related tactile allodynia at any time point, compared with saline (○), over a 2 hr observation period: *y*-axis: 50% paw withdrawal threshold (*PWT*).

To determine whether I_h underlies spontaneous neuronal discharges, we performed extracellular recording *ex vivo* on dorsal root fibers in previously axotomized L4 or L5 excised nerve–DRG preparations. Spontaneous discharges arose from Aβ neurons and some Aδ neurons (distinguished by their conduction velocity) 1–3 weeks after injury. Bath application of 50–100 μM ZD7288 decreased spike frequency in all cases but did not block conduction. Aβ fiber discharges were reduced 91.1 ± 5.6% by 15 min after application. Aδ fiber discharges were also significantly reduced by 44.2 ± 7.7% (Fig. 2). Therefore, frequency of spon-

taneous firing of injured primary afferents is sensitive to the I_h antagonist ZD7288.

We next sought to determine the regulation and molecular identity of the channels mediating I_h in injured neurons. ISH revealed that all neurons appeared to express mRNA for HCN1, HCN2, and HCN3, with HCN1 most abundant. HCN4 hybridization signal could not be readily distinguished from background. This profile is similar to a recent description of normal mouse DRG, with the exception that HCN3 was not detected in the mouse (Moosmang et al., 2001). In DRGs from nerve-ligated rats, ipsilateral to the ligation, we observed marked generalized decreases in both HCN1 and HCN2 mRNA with little change in HCN3 (Fig. 3*a*) compared with the contralateral DRG. Quantitative PCR comparison of the four HCN subtypes in whole L5/6 DRGs confirmed that in sham-operated DRGs the rank order abundance of transcripts is HCN1 ≫ HCN2 > HCN3, HCN4. Using primers flanking the splicing site of intron 1 as judged by alignment with the human genome draft sequence [and see Ludwig et al. (1999)], we saw no differences in HCN1 copy number between control and SNL DRGs. In view of the ISH data, we repeated the study using a second primer pair directed at the same region as the ISH probe (bases 2391–2413 and 2589–2620 of NM 053375); these data showed a statistically significant approximately threefold reduction in post-injury HCN1 transcripts ($p < 0.02$, unpaired t test; $n = 8$ each group). There was a clear and consistent reduction in HCN2 message using both techniques; by PCR, the change was approximately a twofold decrease ($p < 0.02$, unpaired t test; $n = 8$ each group). No significant changes were detected in either HCN3 or HCN4 message (Fig. 3*b*). Thus, changes in the levels of HCN mRNA offer no basis for the observed increases in ZD7288-sensitive spontaneous activity.

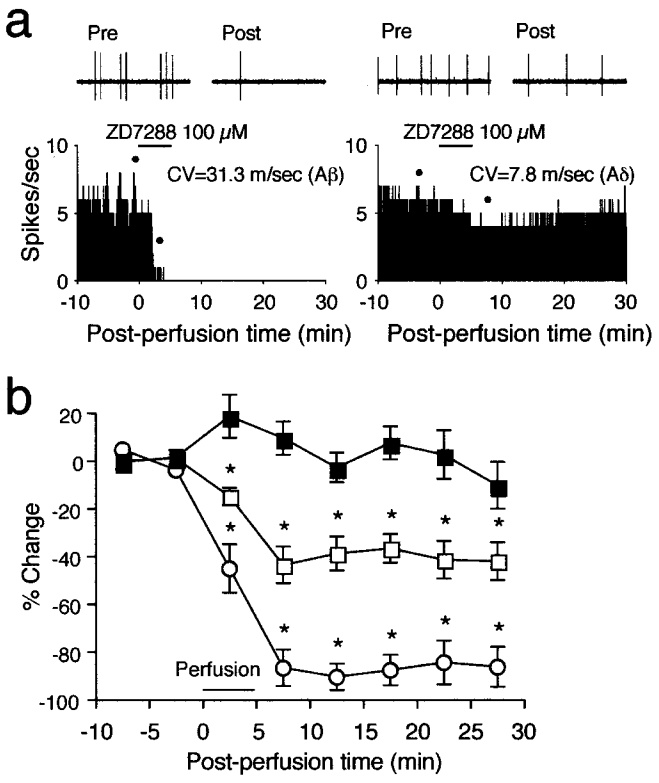

Figure 2. Inhibition of HCN channels suppresses ectopic neuronal discharge without conduction blockade. *a*, Histogram (*y*-axis = spikes/sec) for single fiber *ex vivo* recording from typical fibers before and after application of 100 μM ZD7288. The *left panel* illustrates an Aβ fiber showing complete suppression of ectopic firing 3–4 min after drug application. *Dots* indicate the sources of 1 sec *top panels* showing spike patterns before (*Pre*) and after (*Post*) drug application on a faster time base. The *right panel* similarly illustrates single-fiber recording from a representative Aδ fiber showing attenuation of firing after ZD7288 application. *b*, Time course of percentage change in firing after ZD7288 application: mean ± SEM for seven to eight fibers per group: *filled squares* = ACSF control (Aβ and Aδ fibers combined); *open squares* = Aδ fibers; *open circles* = Aβ fibers. $^*p < 0.05$, one-way ANOVA, Dunnett's multiple comparisons.

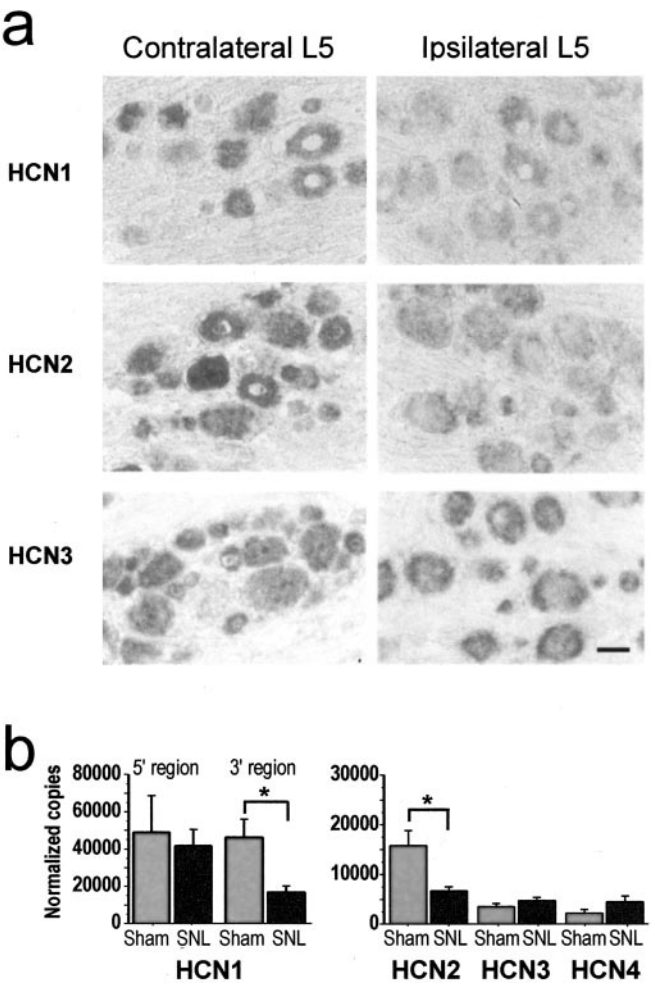

Figure 3. Distribution and quantification of HCN mRNAs after nerve injury. *a*, *In situ* hybridization: comparisons of co-embedded contralateral (uninjured) and ipsilateral (injured) L5 DRGs hybridized with antisense probes for HCN1, HCN2, or HCN3 show a visible reduction in both HCN1 and HCN2 message. No hybridization was seen using sense probes. Scale bar, 50 μm. *b*, Relative quantification of HCN mRNA transcripts in sham versus SNL L5/6 DRGs (normalized copy number per 2 DRGs) by real-time fluorescent quantitative PCR. In the SNL samples, there is a significant reduction in a 3′ but not in a 5′ HCN1 amplicon compared with controls, a significant reduction in HCN2, and no change in HCN3 or HCN4 ($^*p < 0.02$, unpaired *t* test; $n = 8$ each group).

To look for changes in HCN protein levels or subcellular distribution, we characterized proprietary antibodies to the C termini of HCN1 and HCN3 using multiple approaches. Incubation of a fixed HEK293 cell line stably transfected with human HCN1 (HEK–HCN1) with anti-HCN1 revealed strong membrane delineation, whereas no staining was seen in the parent cell line (Fig. 4*a*). The HCN1 antibody recognized a pattern of specific double bands in HEK–HCN1 cell extracts that was absent from extracts of the parent cell line and consistent with the predicted human protein mass of 98.7 kDa (Fig. 4*b*). This pattern was also seen in DRG extracts (see Fig. 7). HCN1 is reported to be glycosylated (Santoro et al., 1997), and similar patterns are recognized for other glycosylated membrane proteins (Luo et al., 2001). The HCN3 antibody recognized

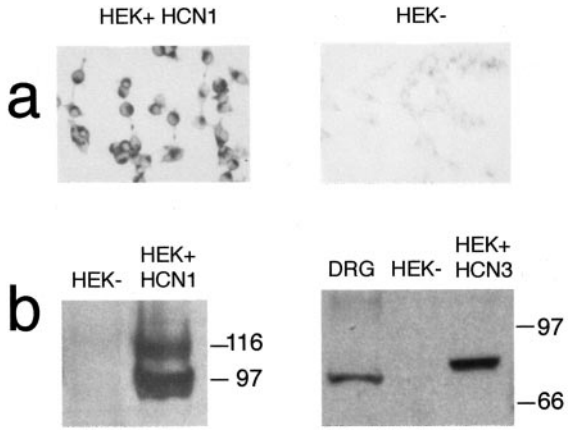

Figure 4. Antibody validation. *a*, Strong immunoreactivity to a stable HEK293–recombinant human HCN1 cell line is seen using anti-HCN1 antibody (*left*, *HEK+HCN1*). Immunoreactivity is absent in the parent (untransfected) cell line (*HEK−*) using the same antibody. *b*, Western blot analysis shows no anti-HCN1 antibody recognition of extracts from untransfected (*HEK−*) cells and a specific double band pattern in HEK+HCN1 cell extracts (*left*). *Right*, Single bands are identified in DRG and stable HEK-tsA201–recombinant human HCN3 (*HEK+HCN3*) cell line extracts using anti-HCN3 antibody, with absence of staining of HEK− cells.

single bands in both stable HEK293–human HCN3 cell line extracts and DRG membranes, consistent with the expected human and rat protein sizes of 86–87 kDa (Fig. 4*b*).

Immunohistochemical staining of adjacent 10 μm sections revealed that HCN1, HCN2, and HCN3 immunoreactivities (IRs) appear colocalized in the membrane region of predominantly, but not exclusively, larger neuronal profiles; HCN4-IR (data not shown) was poorly visualized (Fig. 5). After nerve injury, changes in the distribution of IR mirrored those seen in mRNA levels. Reduced membrane-associated HCN1-IR was seen in large neurons from nerve-ligated rats in comparison with controls (Fig. 6). This decrease in total HCN1-IR was significant after densitometric comparison of bands visualized by Western blot: 10.1 ± 1.1 U (ipsilateral SNL) versus 16.3 ± 1.7 U (contralateral; $p < 0.02$, *t* test) (Fig. 7). Similar results were obtained with a second antibody directed toward the N terminus (data not shown). Marked decreases in HCN2-IR were also apparent in injured DRGs compared with controls, in keeping with the PCR and *in situ* data. Although the distribution of HCN3-IR suggested denser juxtamembranous staining in large neurons after injury, these changes could not be sufficiently resolved at the light microscope level to be considered definitive (Fig. 6), and no change was seen using Western blot analysis.

The observed decreases in HCN mRNA and protein seemed at odds with the behavioral and electrophysiological data. We therefore compared I_h in single, acutely dissociated large neurons from the L5 DRGs of SNL or sham-operated rats using the whole-cell configuration of the patch-clamp method. Nearly all large neurons (diameter 50 ± 1 μm) in both groups expressed I_h currents, as evidenced by their voltage- and time-dependent activation and their sensitivity to 3 mM CsCl (SNL, 98.2 ± 0.6% block, $n = 16$; sham, 99.0 ± 1.0% block, $n = 5$) and 50 μM ZD7288 (SNL 94.6 ± 3.0% block, $n = 9$; sham, 82.7 ± 6.8% block, $n = 4$) (Fig. 8). However, the distribution of current densities measured at −114 mV differed markedly between the two groups of neurons. Current density in controls ranged from 0 to −21.3 pA/pF (normalized to cell capacitance) with a mean of −3.5 ± 0.6 pA/pF ($n = 37$). Most neurons (~58%) expressed less than −4 pA/pF (Fig. 9*a*, *hatched bars*). A striking finding in the SNL neurons was a population shift toward higher I_h current density with a mean of −8.6 ± 0.8 pA/pF ($n = 51$); in contrast to the controls, ~92% expressed I_h more than −4 pA/pF (Fig. 9*a*, *solid bars*). In other words, almost all large neurons in the SNL ganglia showed a high level of I_h expression. Our observations are thus internally consistent with the hypothesis that injured large neurons express more I_h and consequently fire spontaneously, leading to pain responses to light touch, all of which are pharmacologically reversed by an HCN antagonist.

Increased current density elicited by a voltage step to −114

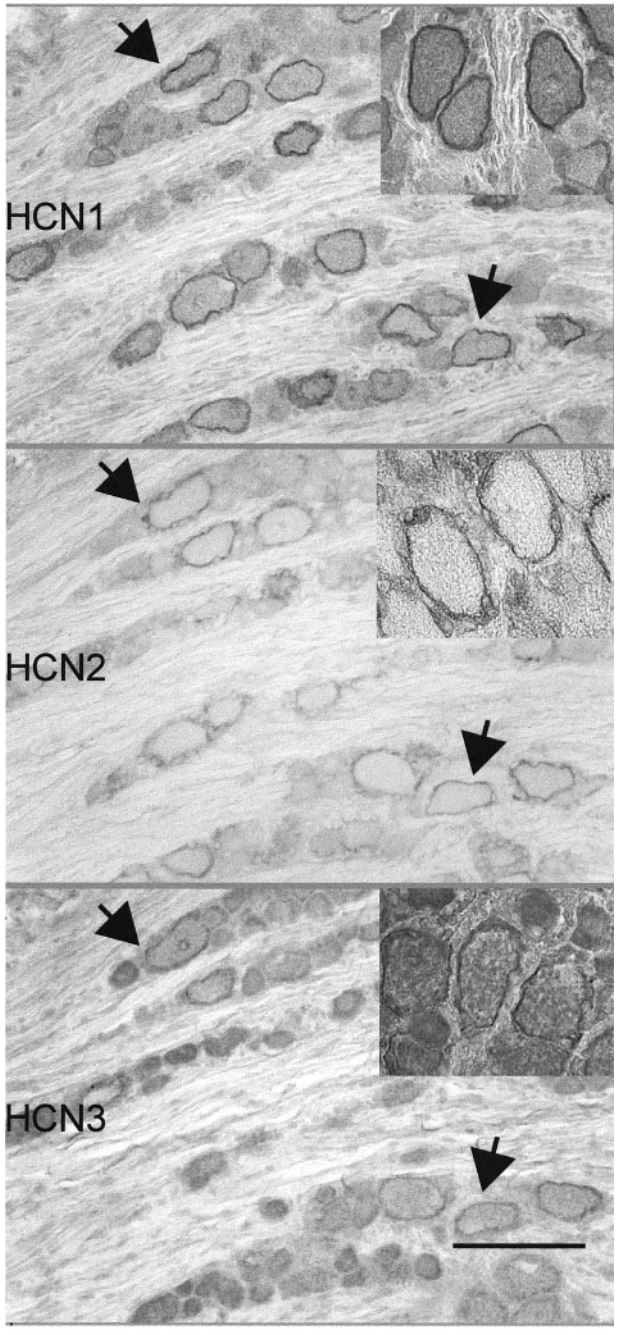

Figure 5. HCN1, HCN2, and HCN3 colocalize in neuronal membranes in DRG. Immunohistochemical visualization of colocalization of HCN1-, HCN2-, and HCN3-IR in neuronal membranes, in adjacent (serial) 10 μm sections from normal DRG, is shown. Colocalization can be seen in numerous neuronal profiles. Immunoreactive profiles are predominantly large neurons. *Arrows* indicate two of the neurons best seen in all sections. Scale bar, 100 μm.

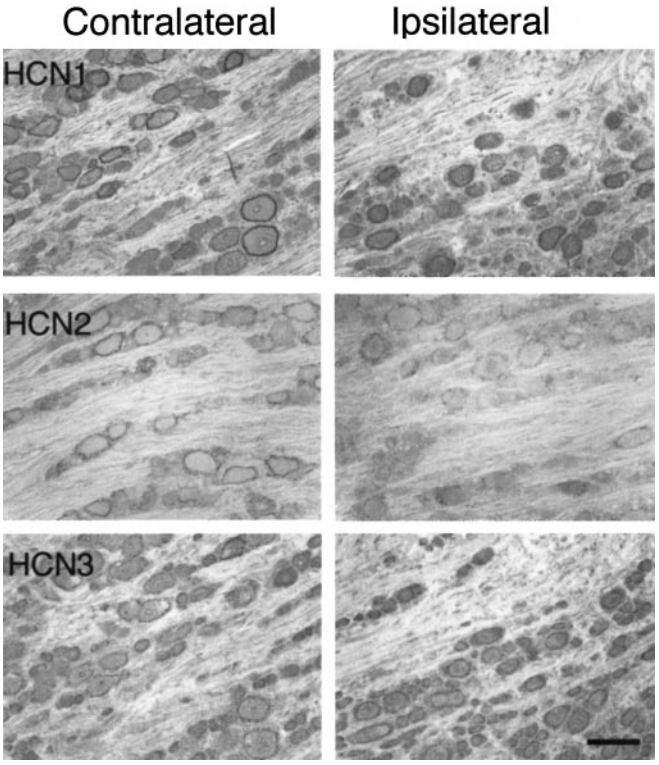

Figure 6. HCN1 and HCN2 membrane IRs are reduced in DRG after nerve injury. Immunohistochemical visualization of HCN1-, HCN2-, and HCN3-IR in simultaneously processed contralateral (uninjured) and ipsilateral (injured) L5 DRGs is shown. Note decreases in HCN1- and HCN2-IR in injured DRG cell membranes. Scale bar, 100 μm.

mV in SNL neurons could result from augmentation of one or more parameters, such as open channel probability (p_o) (e.g., caused by a shift in the voltage dependence of I_h activation), number of functional channels, or single channel conductance. To begin to address these possibilities, we determined the voltage dependence of activation of I_h in control and SNL neurons. Representative recordings from control and SNL ganglia expressing low and high I_h density are shown in Figure 9*b*. Hyperpolarizing voltages more negative than −134 mV appeared to cause membrane breakdown in control neurons that made it difficult to study a wide range of voltage steps in this cell type (Fig. 9*b*, *top left panel*). Interestingly, nerve injury appeared to protect the neurons from apparent membrane breakdown. The midpoint voltage of activation ($V_{0.5}$) of I_h, determined from tail-current analysis after a ≥2 sec test pulse, revealed that $V_{0.5}$ for I_h activation was significantly shifted +8.5 mV in SNL neurons (Fig. 9*c*, Table 1). Consistent with the rightward shift in $V_{0.5}$, the activation threshold in SNL neurons was also significantly more positive (−64.3 ± 1.0 mV; $n = 44$) compared with controls (−73.9 ± 1.9 mV; $n = 35$; $p < 0.001$). Single-channel analysis will be required to determine whether the increase in I_h density is attributable to increases in single-channel conductance or the number of functional channels, or both, and is beyond the scope of this paper.

RMP was significantly more positive in SNL neurons (−64.8 ± 1.0 mV; $n = 22$) compared with controls (−71.9 ± 1.9 mV; $n = 14$; $P < 0.005$). Both control and SNL neurons hyperpolarized after application of ZD7288: −7.8 ± 4.2 mV (sham, $n = 4$), −11.8 ± 3.3 mV (SNL, $n = 5$). There was a tendency for SNL neurons to reveal a larger hyperpolarization compared with sham neurons at similar initial RMP. These experiments were difficult because of the inability to wash out ZD7288 and confirm reversion to baseline. This small data set indicates, importantly, that I_h plays a significant role in the set point of RMP in large DRG neurons and, equally importantly, that other factors additionally contribute to the difference in RMP observed between SNL and control neurons.

Although not always predictive of HCN subunit composition (Franz et al., 2000; Santoro et al., 2000), activation kinetics may give an indication of the expressed HCN isoform, because this parameter is a distinguishing characteristic of the known HCN family members. Therefore, we determined the activation kinetics in sham and SNL neurons. Interestingly, when currents elicited by voltages evoking near-maximal activation were fit by exponential functions, both types of neurons revealed similarly fast activation time constants most consistent with the expression of HCN1 (Table 1). Kinetic differences were only observed near the threshold for activation, consistent with a shift in voltage dependence. Mouse HCN3 reveals a substantially slower activation time constant compared with murine HCN1 (265 vs 30 msec at −140 mV) (Moosmang et al., 2001). Similar results were obtained for human HCN1 and HCN3 at maximally activating voltages when expressed in *Xenopus* oocytes (Table 1).

Discussion

Here we describe for the first time the contribution of augmented I_h to the maintenance of tactile allodynia in a rat model of neuropathic pain. We have used a combination of approaches to comprehensively demonstrate that after nerve injury, augmented I_h clearly sustains both pathological neuronal discharge and pain behavior. Tactile allodynia resulting from tight ligation of the L5/6 spinal nerves was blocked by systemic administration of the I_h antagonist ZD7288. Spontaneous activity in large myelinated fibers, an electrophysiological correlate of pain, was almost com-

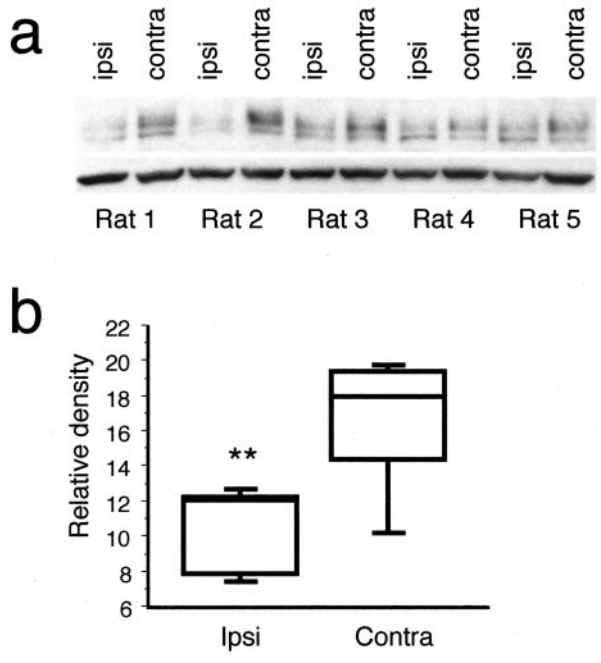

Figure 7. Total HCN1-IR is decreased in DRG after nerve injury. *a*, Western blot analysis was performed on DRGs from five rats 1 week after SNL. Anti-HCN1 antibody was used to compare immunoreactivity in protein extracts from ipsilateral (injured) and contralateral (uninjured) DRGs (*top bands*). Anti-α-tubulin antibody was used to correct for loading errors (*bottom bands*). *b*, Densitometric analysis revealed a significant decrease in HCN1-IR in ipsilateral DRGs compared with contralateral DRGs after normalization to α-tubulin IR. The *box plot* depicts the median and interquartile ranges; *y*-axis = arbitrary density units. $^{**}p < 0.02$, *t* test.

pletely blocked by exposure to ZD7288, suggesting an upregulation of I_h expression in injured large neurons. The proportion of large neurons expressing high I_h density was indeed significantly increased, consistent with I_h contributing to increased ectopic discharges in those cells.

One mechanism underlying enhanced I_h expression in large injured DRG neurons was an increase in p_o, which was manifested as an approximately +10 mV shift in the voltage dependence of activation. Consistent with this finding, the threshold for activation, the kinetics of activation, and the RMP were shifted approximately +10 mV in SNL neurons. The consequences of this may include enhanced electrical excitability attributable to depolarization of the resting potential, faster firing frequencies, and enhanced release of neurotransmitters from central and peripheral terminals. However, the shift in $V_{0.5}$ cannot fully explain the dramatic increase in I_h observed in most DRG neurons, and we are currently investigating the potential contributions of intracellular signaling pathways to the enhanced I_h density. Of note, catecholamine application to injured (but not normal) nerves has been shown to augment spontaneous discharge and pain behavior (Sato and Perl, 1991; Torebjork et al., 1995). In our system, the low abundance of HCN2 and HCN4, the two family members most subject to cyclic nucleotide modulation, decreases the likelihood of a directly cAMP-mediated phenomenon; however, the possibility of HCN-mediated catecholamine responsiveness in this and other pain models remains to be explored.

I_h is described in most normal medium/large acutely dissociated neurons (Scroggs et al., 1994; Abdulla and Smith, 2001). All four HCN subtypes are found in both normal and injured DRGs, with HCN1 the most abundant in both cases. The precise molecular identity of the upregulated I_h in SNL neurons remains unknown because there are presently no isoform-selective pharmacological tools. Despite downregulation of HCN1 protein, I_h in SNL large neurons did not differ significantly from controls with regard to voltage dependence and kinetics of activation, and in both cases best resembled HCN1. One possibility is that altered subunit stoichiometry could underlie the observed functional and molecular differences. Although HCN1, HCN2, and HCN3 appeared to colocalize to soma membranes, the contributions of HCN2 and HCN3 to I_h in these neurons are not clear. Heteromers of HCN1 and HCN2 are reported and result in activation kinetics currents most resembling (but distinguishable from) HCN1, $V_{0.5}$ most resembling HCN2, and intermediate cyclic nucleotide-dependent shifts (Chen et al., 2001; Ulens and Tytgat, 2001). On the other hand, recent evidence indicates that HCN subunits may form heteromeric complexes with non-HCN accessory proteins including MiRP1; differences in accessory proteins could modulate current properties (Yu et al., 2001).

In contrast to the results reported here, Abdulla and Smith (2001) observed a slight decrease in I_h density in large neurons after sciatic nerve transection. This discrepancy may be attributable to the selection of larger cells in the present report and the uniform injury to the DRG created by segmental nerve ligation versus sciatic axotomy, which injures only the ~54% of DRG neurons in L4 and L5 that project an axon to the sciatic nerve (Devor et al., 1985).

Most reports have emphasized the specific nature of the blockade of I_h by ZD7288, noting the absence of effects on other currents or on AP morphology and axonal conduction (Harris and Constanti, 1995; Takigawa et al., 1998; Satoh and Yamada, 2000). BoSmith and colleagues (1993) reported that effects of ZD7288 on other currents, including I_{Ca}, I_k, and the inward rectifier current, were not significant at concentrations that substantially reduced I_h. Other investigators have substantiated these findings (Larkman and Kelly, 2001). However, a recent study describes an I_h-independent "synaptic depression" in rat hippocampal slices caused by ZD7288 as well as DK-AH269, two chemically dissimilar structures, without proposing a mechanism for this observation (Chevaleyre and Castillo, 2002). Our *in vitro* observations were all performed on isolated primary afferent neurons, where synaptic effects are not applicable. Furthermore, the lack of effect of ZD7288 after direct application of a high dose to the spinal cord strongly suggests that nonspecific synaptic effects did not contribute to the behavioral effects of ZD7288.

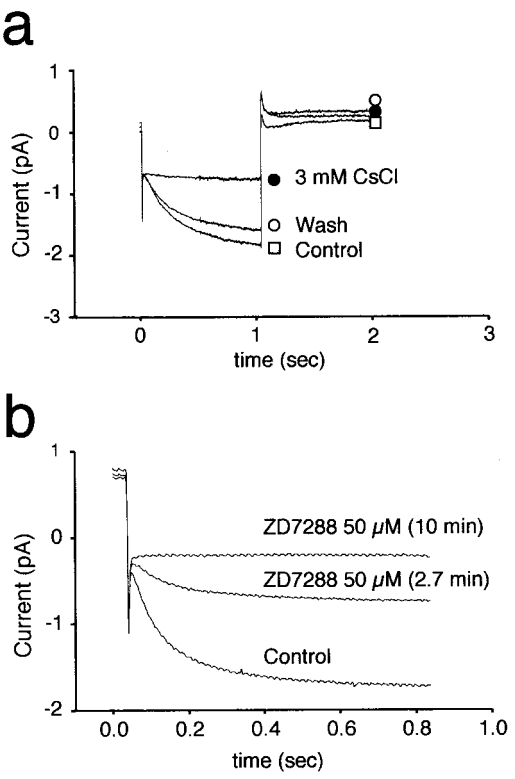

Figure 8. Pharmacological blockade of I_h in dissociated DRG neurons. The pharmacology of hyperpolarization-induced inward currents in large SNL neurons was consistent with that of I_h. Currents were blocked by bath application of 3 mM CsCl (*a*) and 50 μM ZD7288 (*b*). *a*, I_h was elicited by voltage steps from −54 to −114 mV (time 0–1 sec) followed by a step to −54 mV applied every 15 sec. Initially a large slowly developing inward (downward deflection) current was observed after the initial capacitative transient (*Control*, □). After exposure to 3 mM CsCl, the inward current was blocked (*3 mM CsCl*, ●), leaving only a CsCl-insensitive leak current (leak subtraction was not performed in these recordings). The inhibition by CsCl was reversed after washout (*Wash*, ○). *b*, I_h was elicited by voltage steps from −54 to −124 mV applied every 15 sec. Bath application of 50 μM ZD7288 caused a slow onset block of I_h that achieved steady state by 10 min. The effect of ZD7288 was not reversible over 30 min.

Our *in vivo* observations of marked behavioral effects with plasma C_{max} of 3.6 μM are highly consistent with previous reports of the IC_{50} of ZD7288 for I_h. An IC_{50} of ~0.2 μM has been described in guinea pig sinoatrial node cells (BoSmith et al., 1993) and rat facial motoneurons (Larkman and Kelly, 2001). In rat supraoptic neurons, the IC_{50} of ZD7288 was 1.8 μM (Ghamari-Langroudi and Bourque, 2000). Like most investigators, because of the long onset time of ZD7288, we used higher concentrations *in vitro* to speed onset in fragile electrophysiological preparations.

Allodynia is proposed to result from an abnormal processing of low-threshold tactile inputs by spinal mechanisms ("central

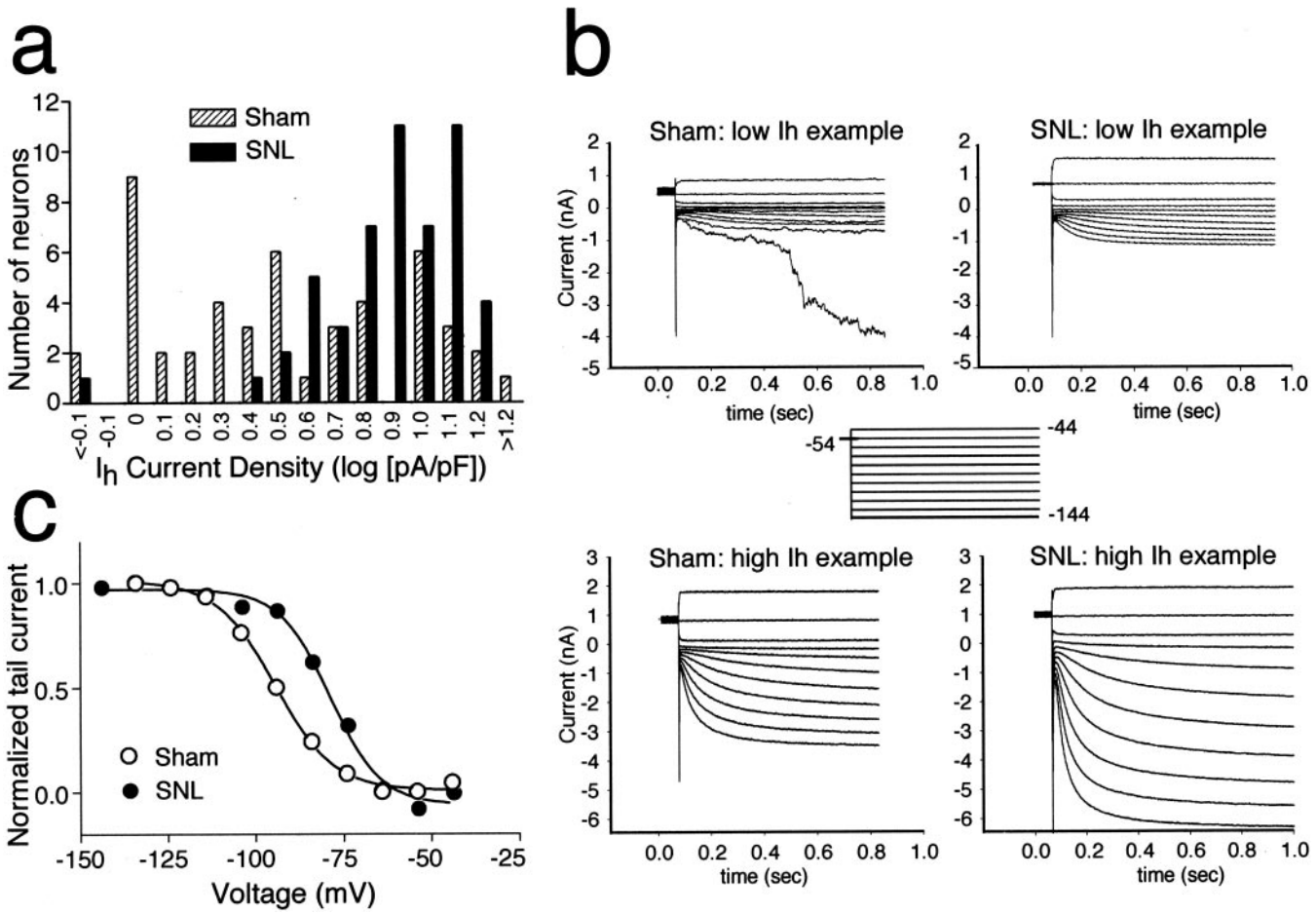

Figure 9. Nerve injury increases I_h density and depolarizes I_h activation threshold. I_h expression in large-diameter rat DRG neurons was increased after ligature of the L5 peripheral nerve (*SNL*). *a*, The distribution of I_h peak current at the end of the test pulse was normalized to cell size (as measured by cell capacitance). I_h was determined in both control (*hatched bars*) and SNL L5 neurons (*solid bars*) at a step to −114 mV. The distribution was skewed toward higher I_h densities in SNL-operated compared with controls. *b*, Examples of families of hyperpolarization-activated currents elicited in sham-injured and injured DRG neurons elicited by the voltage protocol shown in the *inset*. *Top* of *panel* illustrates neurons with low-density I_h as seen in either sham or injured DRGs; *bottom* of *panel* illustrates neurons in both treatment categories with high-density I_h. The number of neurons with abundant I_h was greatly increased after nerve injury. Currents were elicited by −10 mV incremental voltage steps between −44 and −144 mV (*inset*). *c*, Voltage dependence of activation derived from tail current analysis in control and SNL neurons. In SNL neurons, the dependence was shifted to more depolarized potentials (+10 mV) without a significant change in the slope.

sensitization") (Ossipov et al., 2000). Although peripherally applied ZD7288 blocked abnormal spontaneous activity in an isolated nerve/ganglion preparation, blockade of centrally located channels mediating I_h might contribute to the robust antiallodynic effects of systemic ZD7288 in SNL rats. Lumbar intrathecal application of maximum tolerated doses of ZD7288 did not suppress allodynia, arguing that the spinal cord is unlikely to be the site of these effects. Significant expression of HCN channels is documented in supraspinal somatosensory pathways, however, and a role for these higher centers is not excluded by the present work (Monteggia et al., 2000).

A recent study suggests that tetanic stimulation of the mossy fiber–CA1 pathway enhances I_h in presynaptic neurons, which may underlie a presynaptic mechanism of long-term potentiation (Mellor et al., 2002) (but see Chevaleyre and Castillo, 2002). Acute nerve injury generates sustained AP barrages, and the suppression of this barrage has been shown to decrease subsequent pain behavior (Dougherty et al., 1992; Yamamoto et al., 1993)

Table 1. Voltage dependence and kinetics of activation of I_h expressed in different cells

	$V_{0.5}$ (mV)	Slope	τ (msec, @ mV)[a]
Rat SNL neurons	−82.5 ± 2.9 (n = 17)	9.5 ± 1.1 (n = 15)	47.4 ± 1.9 (@ −144 mV)
Rat sham neurons	−91.0 ± 2.6 (n = 14)*	9.3 ± 1.0 (n = 11)	43.4 ± 5.4 (@ −154 mV)
Human HCN1 (oocytes)	−63 ± 4.5 (n = 3)	8.9 ± 0.6 (n = 3)	42.5 ± 9.7 (n = 4), (@ −120 mV)
Human HCN3 (oocytes)	−79.3 ± 1.2 (n = 3)	8.6 ± 0.5 (n = 3)	434 ± 50.5 (n = 3) (@ −130 mV); 378 ± 52.5 (n = 2) (@ −140 mV)

Values shown are the mean ± SEM for the number of cells tested in parentheses. *$p < 0.05$, Student's t test; SNL versus sham neurons.

[a]Fast time constants for exponential fits are shown at equivalent near-maximal voltage steps.

(but see Abdi et al., 2000). In addition, increases in presynaptic I_h have recently been shown to increase synaptic strength by a mechanism that may involve enhanced neurotransmitter release (Beaumont and Zucker, 2000). The possibility that barrage-evoked augmentation of primary afferent I_h plays a role in neuropathic pain bears further investigation.

Much previous work has emphasized the role of sodium channel regulation in the pathogenesis of neuropathic pain and spontaneous discharge (Matzner and Devor, 1994; Okuse et al., 1997; Porreca et al., 1999; Waxman et al., 1999; Boucher et al., 2000). Clearly, sodium channels are critical to the formation of both normal and pathological APs, and expression of unusual or excess sodium channel isoforms may contribute to pathological pain states. Our data contribute to this scenario in that they suggest a specific mechanism for repetitive pacemaker depolarization to the activation threshold of the sodium channel, as well as for the maintenance of an abnormally depolarized RMP, generally contributing to neuronal excitability.

I_h contributes to RMP as well as to spontaneous depolarizations leading to APs in excitable cells. Both properties likely are important in the spontaneous firing seen in the DRG. Our work cannot separate the possibility that firing occurs solely because tonic, I_h-mediated depolarization activates other channels underlying the AP from the possibility that I_h contributes to the subthreshold depolarization phase of the AP to play a pacemaker function. However, Yagi et al. (2000) have shown that in current-clamp mode, ZD7288 (40 μM) blocks the repetitive APs of both normal and injured Aα/β neurons elicited by injection of a depolarizing current pulse, suggesting that I_h is a more important determinant of firing than RMP per se. Of note, in this study, application of ZD7288 also caused hyperpolarization of large neurons, 6.7 $\pm$ 1.9 mV, which is consistent with our results.

Our analysis of neurons in culture revealed a time constant of 45 msec. The sustained spontaneous firing rate of ~5–10 Hz (interspike interval of 100–200 msec) that we documented in our *ex vivo* preparation is fully compatible with a $\tau = 45$ msec. Because we did not observe burst-firing patterns in our preparations, we cannot comment on whether I_h may play a role in the faster firing reported by some authors (Amir et al., 2002). Our recordings were made at standard room temperature, and temperature appears to contribute importantly to the kinetics of HCN channels. A recent study has characterized the Q_{10} of I_h in hippocampal CA1 neurons at 4.5 (Magee, 1998). A $\tau = 45$ msec at 26°C would thus be near 10 msec at 37°C, consistent with a firing rate near 100 Hz and interspike interval of 10 msec. Further studies are required, however, to examine what role I_h plays in rapid burst firing.

In conclusion, spontaneous discharges in DRG neurons have long been thought to sensitize spinal cord neurons and play a deterministic role in ongoing neuropathic pain (Han et al., 2000; C. N. Liu et al., 2000; X. Liu et al., 2000; Na et al., 2000). Our novel findings suggest a specific molecular mechanism underlying the pathophysiology governing alterations in primary afferent function in neuropathic pain syndromes. These findings may enable new therapeutic approaches to both dampen "irritable" nerves and modulate connections to ascending pathways, without loss of normal sensation.

References

Abdi S, Lee DH, Park SK, Chung JM (2000) Lack of pre-emptive analgesic effects of local anaesthetics on neuropathic pain. Br J Anaesth 85:620–623.

Abdulla FA, Smith PA (2001) Axotomy- and autotomy-induced changes in Ca^{2+} and K^+ channel currents of rat dorsal root ganglion neurons. J Neurophysiol 85:644–658.

Amir R, Michaelis M, Devor M (2002) Burst discharge in primary sensory neurons: triggered by subthreshold oscillations, maintained by depolarizing afterpotentials. J Neurosci 22:1187–1198.

Beaumont V, Zucker RS (2000) Enhancement of synaptic transmission by cyclic AMP modulation of presynaptic I_h channels. Nat Neurosci 3:133–141.

BoSmith RE, Briggs I, Sturgess NC (1993) Inhibitory actions of ZENECA ZD7288 on whole-cell hyperpolarization activated inward current (If) in guinea-pig dissociated sinoatrial node cells. Br J Pharmacol 110:343–349.

Boucher TJ, Okuse K, Bennett DLH, Munson JB, Wood JN, McMahon SB (2000) Potent analgesic effects of GDNF in neuropathic pain states. Science 290:124–127.

Braissant O, Wahli W (1998) A simplified *in situ* hybridization protocol using non-radioactively labelled probes to detect abundant and rare mRNAs on tissue sections. Biochemica 1:10–16.

Burchiel KJ (1984) Spontaneous impulse generation in normal and denervated dorsal root ganglia: sensitivity to alpha-adrenergic stimulation and hypoxia. Exp Neurol 85:257–272.

Chaplan SR, Bach FW, Pogrel JW, Chung JM, Yaksh TL (1994) Quantitative assessment of allodynia in the rat paw. J Neurosci Methods 53:55–63.

Chen S, Wang J, Siegelbaum SA (2001) Properties of hyperpolarization-activated pacemaker current defined by coassembly of HCN1 and HCN2 subunits and basal modulation by cyclic nucleotide. J Gen Physiol 117:491–504.

Chevaleyre V, Castillo PE (2002) Assessing the role of I_h channels in synaptic transmission and mossy fiber LTP. Proc Natl Acad Sci USA 99:9538–9543.

Devor M, Govrin-Lippmann R, Frank I, Raber P (1985) Proliferation of primary sensory neurons in adult rat dorsal root ganglion and the kinetics of retrograde cell loss after sciatic nerve section. Somatosens Res 3:139–167.

Dougherty PM, Garrison CJ, Carlton SM (1992) Differential influence of local anesthetic upon two models of experimentally induced peripheral mononeuropathy in the rat. Brain Res 570:109–115.

Dubin AE, Bahnson T, Weiner JA, Fukushima N, Chun J (1999a) Lysophosphatidic acid stimulates neurotransmitter-like conductance changes that precede GABA and L-glutamate in early, presumptive cortical neuroblasts. J Neurosci 19:1371–1381.

Dubin AE, Huvar R, D'Andrea MR, Pyati J, Zhu JY, Joy KC, Wilson SJ, Galindo JE, Glass CA, Luo L, Jackson MR, Lovenberg TW, Erlander MG (1999b) The pharmacological and functional characteristics of the serotonin 5-HT(3A) receptor are specifically modified by a 5-HT(3B) receptor subunit. J Biol Chem 274:30799–30810.

Franz O, Liss B, Neu A, Roeper J (2000) Single-cell mRNA expression of HCN1 correlates with a fast gating phenotype of hyperpolarization-activated cyclic nucleotide-gated ion channels (Ih) in central neurons. Eur J Neurosci 12:2685–2693.

Ghamari-Langroudi M, Bourque CW (2000) Excitatory role of the hyperpolarization-activated inward current in phasic and tonic firing of rat supraoptic neurons. J Neurosci 20:4855–4863.

Govrin-Lippmann R, Devor M (1978) Ongoing activity in severed nerves: source and variation with time. Brain Res 159:406–410.

Han HC, Lee DH, Chung JM (2000) Characteristics of ectopic discharges in a rat neuropathic pain model. Pain 84:253–261.

Harper AA, Lawson SN (1985) Conduction velocity is related to morphological cell type in rat dorsal root ganglion neurones. J Physiol (Lond) 359:31–46.

Harris NC, Constanti A (1995) Mechanism of block by ZD 7288 of the hyperpolarization-activated inward rectifying current in guinea pig substantia nigra neurons in vitro. J Neurophysiol 74:2366–2378.

Ishii TM, Takano M, Ohmori H (2001) Determinants of activation kinetics in mammalian hyperpolarization-activated cation channels. J Physiol (Lond) 537:93–100.

Kajander KC, Bennett GJ (1992) Onset of a painful peripheral neuropathy in rat: a partial and differential deafferentation and spontaneous discharge in A beta and A delta primary afferent neurons. J Neurophysiol 68:734–744.

Kaupp UB, Seifert R (2001) Molecular diversity of pacemaker ion channels. Annu Rev Physiol 63:235–257.

Kim SH, Chung JM (1992) An experimental model for peripheral neurop-

athy produced by segmental spinal nerve ligation in the rat. Pain 50:355–363.
Larkman PM, Kelly JS (2001) Modulation of the hyperpolarisation-activated current, Ih, in rat facial motoneurones in vitro by ZD-7288. Neuropharmacology 40:1058–1072.
Lee DH, Liu X, Kim HT, Chung K, Chung JM (1999) Receptor subtype mediating the adrenergic sensitivity of pain behavior and ectopic discharges in neuropathic Lewis rats. J Neurophysiol 81:2226–2233.
Liman ER, Tytgat J, Hess P (1992) Subunit stoichiometry of a mammalian K^+ channel determined by construction of multimeric cDNAs. Neuron 9:861–871.
Liu CN, Wall PD, Ben-Dor E, Michaelis M, Amir R, Devor M (2000) Tactile allodynia in the absence of C-fiber activation: altered firing properties of DRG neurons following spinal nerve injury. Pain 85:503–521.
Liu X, Eschenfelder S, Blenk KH, Janig W, Habler H (2000) Spontaneous activity of axotomized afferent neurons after L5 spinal nerve injury in rats. Pain 84:309–318.
Ludwig A, Zong X, Jeglitsch M, Hofmann F, Biel M (1998) A family of hyperpolarization-activated mammalian cation channels. Nature 393:587–591.
Ludwig A, Zong X, Stieber J, Hullin R, Hofmann F, Biel M (1999) Two pacemaker channels from human heart with profoundly different activation kinetics. EMBO J 18:2323–2329.
Luo ZD, Chaplan SR, Higuera ES, Sorkin LS, Stauderman KA, Williams ME, Yaksh TL (2001) Upregulation of dorsal root ganglion (alpha)2(delta) calcium channel subunit and its correlation with allodynia in spinal nerve-injured rats. J Neurosci 21:1868–1875.
Magee JC (1998) Dendritic hyperpolarization-activated currents modify the integrative properties of hippocampal CA1 pyramidal neurons. J Neurosci 18:7613–7624.
Matzner O, Devor M (1994) Hyperexcitability at sites of nerve injury depends on voltage-sensitive Na^+ channels. J Neurophysiol 72:349–359.
Mayer ML, Westbrook GL (1983) A voltage-clamp analysis of inward (anomalous) rectification in mouse spinal sensory ganglion neurones. J Physiol (Lond) 340:19–45.
Mellor J, Nicoll RA, Schmitz D (2002) Mediation of hippocampal mossy fiber long-term potentiation by presynaptic Ih channels. Science 295:143–147.
Monteggia LM, Eisch AJ, Tang MD, Kaczmarek LK, Nestler EJ (2000) Cloning and localization of the hyperpolarization-activated cyclic nucleotide-gated channel family in rat brain. Brain Res Mol Brain Res 81:129–139.
Moosmang S, Stieber J, Zong X, Biel M, Hofmann F, Ludwig A (2001) Cellular expression and functional characterization of four hyperpolarization-activated pacemaker channels in cardiac and neuronal tissues. Eur J Biochem 268:1646–1652.
Na HS, Ko KH, Back SK, Sung B, Yoo DJ, Hong SK (2000) Role of signals from the dorsal root ganglion in neuropathic pain in a rat model. Neurosci Lett 288:147–150.
Okuse K, Chaplan SR, McMahon SB, Luo ZD, Calcutt NA, Scott BP, Akopian AN, Wood JN (1997) Regulation of expression of the sensory neuron-specific sodium channel SNS in inflammatory and neuropathic pain. Mol Cell Neurosci 10:196–207.
Olsson Y (1968) Topographical differences in the vascular permeability of the peripheral nervous system. Acta Neuropathol (Berl) 10:26–33.
Olsson Y (1971) Studies on vascular permeability in peripheral nerves. IV. Distribution of intravenously injected protein tracers in the peripheral nervous system of various species. Acta Neuropathol (Berl) 17:114–126.
Ossipov MH, Lai J, Malan Jr TP, Porreca F (2000) Spinal and supraspinal mechanisms of neuropathic pain. Ann NY Acad Sci 909:12–24.
Pape HC (1996) Queer current and pacemaker: the hyperpolarization-activated cation current in neurons. Annu Rev Physiol 58:299–327.
Porreca F, Lai J, Bian D, Wegert S, Ossipov MH, Eglen RM, Kassotakis L, Novakovic S, Rabert DK, Sangameswaran L, Hunter JC (1999) A comparison of the potential role of the tetrodotoxin-insensitive sodium channels, PN3/SNS and NaN/SNS2, in rat models of chronic pain. Proc Natl Acad Sci USA 96:7640–7644.
Rappaport ZH, Devor M (1990) Experimental pathophysiological correlates of clinical symptomatology in peripheral neuropathic pain syndromes. Stereotact Funct Neurosurg 55:90–95.
Ritter AM, Mendell LM (1992) Somal membrane properties of physiologically identified sensory neurons in the rat: effects of nerve growth factor. J Neurophysiol 68:2033–2041.
Santoro B, Tibbs GR (1999) The HCN gene family: molecular basis of the hyperpolarization-activated pacemaker channels. Ann NY Acad Sci 868:741–764.
Santoro B, Grant SG, Bartsch D, Kandel ER (1997) Interactive cloning with the SH3 domain of N-src identifies a new brain specific ion channel protein, with homology to eag and cyclic nucleotide-gated channels. Proc Natl Acad Sci USA 94:14815–14820.
Santoro B, Liu DT, Yao H, Bartsch D, Kandel ER, Siegelbaum SA, Tibbs GR (1998) Identification of a gene encoding a hyperpolarization-activated pacemaker channel of brain. Cell 93:717–729.
Santoro B, Chen S, Luthi A, Pavlidis P, Shumyatsky GP, Tibbs GR, Siegelbaum SA (2000) Molecular and functional heterogeneity of hyperpolarization-activated pacemaker channels in the mouse CNS. J Neurosci 20:5264–5275.
Sato J, Perl ER (1991) Adrenergic excitation of cutaneous pain receptors induced by peripheral nerve injury. Science 251:1608–1610.
Satoh TO, Yamada M (2000) A bradycardiac agent ZD7288 blocks the hyperpolarization-activated current (I(h)) in retinal rod photoreceptors. Neuropharmacology 39:1284–1291.
Scroggs RS, Todorovic SM, Anderson EG, Fox AP (1994) Variation in IH, IIR, and ILEAK between acutely isolated adult rat dorsal root ganglion neurons of different size. J Neurophysiol 71:271–279.
Shir Y, Seltzer Z (1990) A-fibers mediate mechanical hyperesthesia and allodynia and C-fibers mediate thermal hyperalgesia in a new model of causalgiform pain disorders in rats. Neurosci Lett 115:62–67.
Takigawa T, Alzheimer C, Quasthoff S, Grafe P (1998) A special blocker reveals the presence and function of the hyperpolarization-activated cation current IH in peripheral mammalian nerve fibres. Neuroscience 82:631–634.
Torebjork E, Wahren L, Wallin G, Hallin R, Koltzenburg M (1995) Noradrenaline-evoked pain in neuralgia. Pain 63:11–20.
Ulens C, Tytgat J (2001) Functional heteromerization of HCN1 and HCN2 pacemaker channels. J Biol Chem 276:6069–6072.
Waddell PJ, Lawson SN (1990) Electrophysiological properties of subpopulations of rat dorsal root ganglion neurons in vitro. Neuroscience 36:811–822.
Waxman SG, Dib-Hajj S, Cummins TR, Black JA (1999) Sodium channels and pain. Proc Natl Acad Sci USA 96:7635–7639.
Yagi J, Hirai N, Sumino R (2000) Action of the hyperpolarization-activated current blocker ZD7288 in dorsal root ganglion neurons classified by conduction velocity. In: Proceedings of the 9th World Congress on Pain (Devor M, Rowbotham MC, Wiesenfeld-Hallin Z, eds), pp 109–117. Seattle: IASP.
Yaksh TL, Rudy TA (1976) Chronic catheterization of the spinal subarachnoid space. Physiol Behav 17:1031–1036.
Yamamoto T, Shimoyama N, Mizuguchi T (1993) Role of the injury discharge in the development of thermal hyperesthesia after sciatic nerve constriction injury in the rat. Anesthesiology 79:993–1002.
Yu H, Wu J, Potapova I, Wymore RT, Holmes B, Zuckerman J, Pan Z, Wang H, Shi W, Robinson RB, El-Maghrabi MR, Benjamin W, Dixon J, McKinnon D, Cohen IS, Wymore R (2001) MinK-related peptide 1: a beta subunit for the HCN ion channel subunit family enhances expression and speeds activation. Circ Res 88:E84–87.